Methods and Technologies for the Implementation of Large-Scale Robot Tactile Sensors

Alexander Schmitz, Perla Maiolino, Marco Maggiali, Lorenzo Natale, Giorgio Cannata, and Giorgio Metta

***Abstract*—Even though the sense of touch is crucial for humans, most humanoid robots lack tactile sensing. While a large number of sensing technologies exist, it is not trivial to incorporate them into a robot. We have developed a compliant "skin" for humanoids that integrates a distributed pressure sensor based on capacitive technology. The skin is modular and can be deployed on nonflat surfaces. Each module scans locally a limited number of tactile-sensing elements and sends the data through a serial bus. This is a critical advantage as it reduces the number of wires. The resulting system is compact and has been successfully integrated into three different humanoid robots. We have performed tests that show that the sensor has favorable characteristics and implemented algorithms to compensate the hysteresis and drift of the sensor. Experiments with the humanoid robot iCub prove that the sensors can be used to grasp unmodeled, fragile objects.**

***Index Terms*—Capacitance measurement, force and tactile sensing, grasping, humanoid robots, robot tactile systems.**

I. Introduction

THE lack of sensitive skin for robots has proven to be a key limitation preventing human-like performance in tasks that require controlled physical interactions in uncontrolled environments. Tactile sensing is crucial for safe interactions of robots with humans and objects, because contact sensing provides the most direct feedback to control contact forces both in voluntary and involuntary interactions with the environment. Beyond classical robot-interaction tasks (e.g., the peg-in-hole problem), where the contact is expected and planned to occur at specific locations of the robot, more advanced applications require more complex forms of interactions: the location and the characteristics of the contact cannot be predicted or modeled in advance. Therefore, a tactile sensor system is required, which is capable of measuring contact forces over large areas.

Tactile sensing in robotics has been widely investigated over the past 30 years [1]. Research in this field has focused largely on transduction principles and transduction technologies [2]; however, various technical issues have limited the transition from a single tactile element (or a small matrix prototype) to a large-scale integrated solution: A sensitive robot skin should be formed by many spatially distributed sensing points and cannot be achieved by simply aggregating manually a large number of single elements. Embedded electronics and distributed computation are necessary to facilitate the integration in the robot; otherwise, an overwhelming amount of wires would impede the dexterity of the robot. The system should be modular, and it should be simple to tailor the sensor system to the various shapes of the surface of humanoid robots. Moreover, due to the repeated contacts with the environment, the robotic skin will get more often damaged than other robots parts; therefore, faulty skin parts should be easy to repair or replace. Especially, if the system is intended to be produced in large numbers, the ease and speed of production have to be taken into account, and off-the-shelf components should be used to decrease the costs.

Several tactile systems have been integrated into humanoid robots and described in the literature (a representative selection of them will be presented in the next section). Some of them are modular and include hierarchical data processing. Yet, the modules are usually big and cannot be installed on small robot parts; furthermore, in many cases, the spatial resolution is low, or the modules cannot communicate between themselves and need to be individually connected to a control board. Instead, small sensor modules are necessary (therefore, even small microcontrollers would be too big) that can also communicate between themselves (therefore, locally integrated multiplexers are not sufficient).

In this paper, we present a tactile-sensing system based on relatively small, bendable, and serially interconnected modules. They form a conformable mesh of sensors and provide pressure measurements and information about the contact locations between the robot and the environment. Each module features 12 capacitive taxels and includes a small commercially available analog-to-digital converter [3]. Moreover, in most cases, the modules have a triangular shape (where all sides are 3 cm long). Each triangle has three communication ports placed along its sides for communication with adjacent triangles. This way, they are connected to each other in order to create a networked

Manuscript received January 13, 2011; revised January 13, 2011; accepted March 16, 2011. Date of publication May 24, 2011; date of current version June 9, 2011. This paper was recommended for publication by Associate Editor K. Hosoda and Editor W. K. Chung upon evaluation of the reviewers' comments. This work was supported by the European Community's Seventh Framework Programme (FP7/20072013) under Grant 231500 (project *ROBOSKIN*) and Grant 215843 (project *Poeticon*).

A. Schmitz is with the Department of Robotics, Brain and Cognitive Sciences, Italian Institute of Technology, 16163 Genova, Italy, and also with the Department of Automatic Control and Systems Engineering, University of Sheffield, Sheffield, S1 3JD, U.K. (e-mail: alexander.schmitz@iit.it).

P. Maiolino and G. Cannata are with the Dipartimento di Informatica Sistemistica e Telematica, Universita degli Studi di Genova, 16145 Genova, Italy (e-mail: perla.maiolino@unige.it; giorgio.cannata@unige.it).

M. Maggiali and L. Natale are with the Department of Robotics, Brain and Cognitive Sciences, Italian Institute of Technology, 16163 Genova, Italy (e-mail: marco.maggiali@iit.it; lorenzo.natale@iit.it).

G. Metta is with the Department of Robotics, Brain and Cognitive Sciences, Italian Institute of Technology, 16163 Genova, Italy, and also with the Dipartimento di Informatica Sistemistica e Telematica, Universita degli Studi di Genova, 16145 Genova, Italy (e-mail: giorgio.metta@iit.it).

Color versions of one or more of the figures in this paper are available online at http://ieeexplore.ieee.org.

Digital Object Identifier 10.1109/TRO.2011.2132930

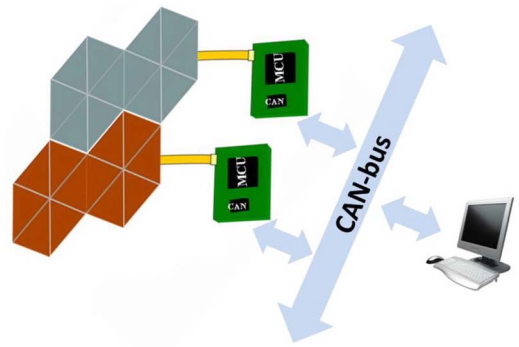

Fig. 1. Network structure. The triangles communicate over an inter-integrated circuit (I^2C) serial bus. Only one out of 16 needs to be connected to the MTB, which sends the measurements over a controller area network (CAN bus).

structure (Patent No. I0128764). The measurements are sent to a microcontroller board (MTB), which can control and collect the measurements from up to 16 modules (see Fig. 1). From the manufacturing point of view, the triangular modules are produced as large interconnected sheets of flexible printed circuit boards (PCBs). The sheets can be cut along the interconnection ports to form various shapes. As a result, the system has the following benefits.

1) *Modularity*: The system consists, at the lowest level, of relatively small and flexible modules, which enhances the conformability to different shapes. Modules can be easily added or removed to account for deliberate changes or to replace broken ones. The triangular modules can be interconnected and networked to achieve larger sensing surfaces and conform to various shapes.
2) *Portability*: The methods and technologies are platform-independent in order to enhance portability to different robotic platforms. This is demonstrated by the fact that the skin has been installed on three robots: iCub, NAO, and KASPAR. Just minimal changes between the implementations on the different robots were necessary, which are described in Section IV. Only for the fingertips of the robot iCub, we had to design a specific solution, due their very small size and high curvature. Yet, even in this case, the same capacitive technology and the same basic structure of the transducer could be used. This demonstrates that the sensor can be customized to cover even smaller robot parts if necessary.
3) *Producibility*: The construction of the sensor is relatively fast, simple, and cheap. This allows implementing large-scale robot skin systems, using state of the art technologies and accessible servicing facilities, which can be tailored for different robotic platforms. The general implementation steps are reported in Section IV, thus giving the interested reader the possibility to reproduce them.

Moreover, a layer of silicone foam covers the entire skin, thus protecting both the sensors and the robot. In addition, low power consumption is important for autonomous robots; our system uses only about 5 W/m^2.

The rest of this paper is organized as follows. Section II gives an overview of existing approaches to tactile sensing, especially for humanoid robots. Section III describes the sensors we have developed. Section IV presents the implementation of the sensors on three different robots. Sections V and VI show the characteristics of the sensor, for example, its drift, noise, spatial resolution, and sensitivity. Moreover, we present compensation algorithms for baseline drift and hysteresis, which commonly affect capacitive pressure sensors. Section VII describes an experiment we have performed to evaluate the ability of the sensor to aid grasping. Finally, Section VIII presents the conclusion and future work.

II. Previous Work

A. Large-Scale Tactile Sensors for Humanoids

One of the first examples of a conformable and truly scalable robot skin system was proposed by Ohmura *et al.* [4]. They presented self-contained modules, which are based on a tree-shaped flexible PCB with integrated digitization. Yet, because microcontrollers are used and due to the shape of the PCB, the modules are too big for small robot parts, and the spatial resolution is limited [5]. The tactile system that has been developed for the robot RI-MAN also uses flexible PCBs with a tree-like shape to conform to curved surfaces [6]. The tactile elements are commercially available piezoresistive semiconductor pressure sensors, and the measurements show less hysteresis than those of Ohmura *et al.* To reduce the number of wires, the sensor modules include multiplexers, but this approach requires each module to be connected individually to a controller board.

The robot ARMAR-III [7] uses skin patches based on piezoresistive sensor matrices with embedded multiplexers. The patches have a flat or a cylindrical shape and are specifically designed for the different parts of the robot; smaller patches are used for the fingers. In Kotaro [8], tactile sensing is achieved by using flexible bandages formed by two flexible PCBs with an intermediate layer of pressure-sensitive conductive rubber. Each bandage has 64 taxels, but no integrated data-acquisition electronics are mentioned. Piezoelectric transducers are used for the humanoid robots Robovie-IIS [9] and CB2 [10]. The transducers were placed individually on the robots and the sensitive skin has a limited spatial resolution.

B. Stretchable Sensors

Another challenge is the development of sensors that are not only bendable but stretchable as well. This would increase the conformability to compound curved shapes, and they could also be used to cover joints. A stretchable, flexible, large-area "E-skin" that is formed by a net-like structure is presented in [11]. According to the authors, issues of the perforated configuration are that the sensor array cannot be stretched biaxially or in all directions, and the stretchability is limited to 25%–30% because the utilized materials are not inherently stretchable. In addition, in [12], a stretchable tactile distribution sensor is presented. The authors also tackled the problem of the sensitivity to stretch: pressure-sensitive stretch-insensitive material was developed. The resulting structure can be stretched to around 140% of its original size in both directions and can cover, for

example, a human elbow. A drawback of the sensor is the relatively high power consumption. While no large-scale integration of such sensors has been performed yet, it would be interesting to implement them in the future above the joints of robots.

C. Skin Sensors for Robot Hands

Only a limited number of dexterous robotic hands incorporate skin sensors. The GIFU hand III [13] includes a tactile sensor with 859 taxels. In addition, it has commercial six-axis force–torque sensors in the fingertips. The skin is based on pressure-sensitive piezo-resistive ink, which is is only 0.2-mm thick and can conform to flat and cylindrical shapes. It includes no local data processing and the sensor cables from all the transducers are routed along the fingers and the palm. Moreover, the skin is not compliant. The sensors in the MAC hand [14] are modular with embedded electronics. Each module includes a three-axis force sensor and sensitive skin with 64 taxels based on pressure-sensitive rubber. The modules are relatively big. The Obrero hand [15] has 40 contact points that embed four Hall-effect sensors each. Tactile sensors based on quantum tunneling composite (QTC) have been incorporated in the Shadow hand [16] and the Robonaut hand [17]. However, little information concerning the performance of this technology has been published.

D. Touch Sensors Based on Capacitive Technology

Capacitive sensors cannot only be used to detect pressure, but, for example, in [18], a three-axis sensor is proposed. In [19] and [20], sensor matrices with very high spatial resolutions are reported. In [21], an artificial skin based on capacitive technology with interesting characteristics, like no apparent hysteresis and low noise, is presented. However, these solutions have not been integrated into a robotic system. A tactile system based on capacitive sensing was developed for the robot Paro [22]. A system using small brushes of fibers mounted on a diaphragm was integrated into a robot gripper, thereby resulting in high sensitivity [23].

Pressure profile systems [24] sells capacitive pressure sensors. The "RoboTouch" system has been included in the robots PR2 [24] and Twendy-One [25]. Twendy-One has 241 pressure-sensing points based on capacitive technology in each of its hands and 134 sensor points on its arm and upper body. Moreover, the skin is compliant and the fingertips have a round shape as well as include a six-axis force sensor. However, to the best of our knowledge, no data has been published concerning the performance of these sensors.

The concept of the sensor system used in this paper was first introduced in [26]. The fingertips were described in detail in [27]. The integration on the robotic hands and a comparison of the characteristics of the fingertips and the palm was presented in [28]. In [29], first grasping experiments were performed with the help of the sensor system. In this paper, we show the implementation of the skin on different body parts and on diverse robots. New experimental results, algorithms for hysteresis, and drift compensation and grasping with tactile feedback are presented.

III. Capacitive Pressure Sensor

We designed a "skin" to cover the surface of humanoid robots. It incorporates a distributed pressure sensor based on capacitive technology. The transducer consists of a soft dielectric sandwiched by electrodes. When pressure is applied to the sensor, the distance between the electrodes above and below the dielectric changes, and the capacitance changes accordingly (i.e., capacitance is a function of distance).

The basis of the sensor is a flexible PCB. It includes the electronics to obtain 12 measurements of capacitance and send them over a serial bus. In particular, each PCB includes 12 round pads, i.e., one for each taxel, and a capacitance-to-digital converter (CDC) (AD7147 from *Analog Devices* [3]). The chip can measure the capacitance of all taxels with 16-bit resolution; however, in our implementation, three bits are affected by noise and five bits are out of range. Therefore, we use only 8-bit measurements, for which one measurement unit corresponds to 2.88 fF. The CDC has an I^2C serial interface and up to four chips can communicate over the same serial line.

The shape of the PCB is, in most cases, a triangle (only for the fingertips of the robot iCub we used a unique solution, which we will discuss later). It is an equilateral triangle; the edges are 30-mm long, and the altitude is 26 mm. The triangular PCBs also include the electronics to communicate between themselves: three communications ports placed along the sides of the triangle relay the signals from one triangle to the adjacent ones. Up to 16 triangles can be connected in this way (four serial buses with four different addresses each), and only one of them needs to be connected to an MTB. This is a critical advantage since it reduces the amount of wires and electrical connections that are required. Moreover, the MTB is small (i.e., 17.4×25.5 mm).

The CDC chip works internally at 250 kHz, and the measurements sent from the CDC chip are the result of an averaging process. In particular, the MTB can be used to program each CDC to deliver individual measurements for each taxel at about 25, 50, or 100 Hz. It is also possible to average spatially, i.e., it is possible to obtain an average of all 12 taxels at about 500 Hz.

Above the flexible PCB is a layer of silicone foam (Soma Foama 15 from *Smooth-On*). It is 2-mm thick for the hands of the robot iCub and 3-mm thick in all other cases. It covers the 12 pads and acts as a deformable dielectric for the capacitive pressure sensor. The foam makes the skin compliant as well.

For the hands of iCub, on top of the silicone foam, there is a second conductive layer: electrically conductive Lycra-like material for the palms and electrically conductive silicone for the fingertips (see Section IV-B). This layer is connected to ground and enables the sensor to respond to objects irrespective of their material. It serves as the common electrode above the silicone foam for all the taxels. When pressure is applied to the sensor, this layer gets closer to the round pads on the PCB and the sensor measures the distance. This layer also reduces the electronic noise coming from the environment, in particular, the stray capacity, which can be a problem for capacitive pressure sensor systems [30].

For the lower arms of iCub and the other humanoids, we do not use a conductive layer on top of the silicone foam, as in

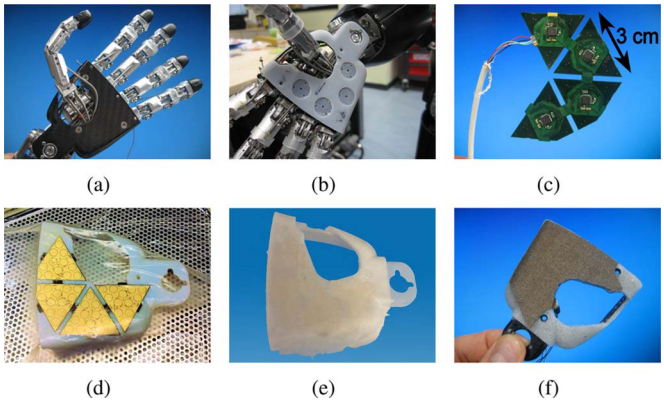

Fig. 2. Production steps for the palm of iCub. (a) Palm without the sensor. (b) Support with shallow round holes that provide space for the CDC chips. (c) Mesh of triangles for the palm. The PCBs are shown from the back and their size is indicated. (d) Triangles are bonded onto the support. (e) Palm with the dielectric silicone foam layer. (f) Finished palm with the conductive Lycra-like material.

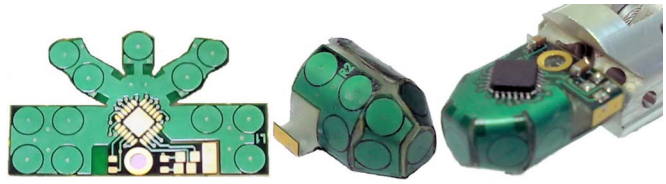

Fig. 3. Flexible PCB for the fingertips. (Left) Twelve pads for the capacitive pressure sensor system and the soldering points for the CDC chip, for two capacitors, and for the connector cables for the digital output are visible. (Middle) Flexible PCB wrapped around the inner support can be seen. The inner support is produced with a 3-D printer. (Right) Flexible PCB wrapped around the inner support and mounted on the last phalange of the finger can be seen. The AD7147 chip and the capacitors are soldered on the PCB.

these cases, the robot is intended to interact only with humans, and in that case, the human constitutes the ground plane (like in many consumer products, which are responsive to humans, but are not responsive to insulators, for example).

IV. Implementation of Artificial Skin on Three Different Robots (i.e., iCub, KASPAR, and NAO)

The artificial skin has been implemented on three robots: iCub, KASPAR, and NAO. The three robots have different sizes and shapes, and the tactile feedback will be used for different purposes. Nevertheless, the methods that have been used to implement the artificial skin were nearly the same, which demonstrates the portability of the sensor system.

iCub is a humanoid robot with the size of a 3.5-year-old child [31]. To enable the robot to grasp and manipulate objects, touch sensors have been integrated into its hands [29]. Tactile fingertips are particularly important for such tasks. Furthermore, another target was to cover the lower arms with the artificial skin to enable humans to provide corrective touch feedback, which is used to indicate position adjustments [32].

KASPAR is a child-sized humanoid robot [33]. It is used to study human–robot interaction and to investigate the possible use of robotic systems as therapeutic and educational tools. In particular, the robot is used to encourage autistic children to engage in social interactions. In order to improve the interaction possibilities with the children, the target was to cover the hands, the arms, the cheeks, the feet, and the torso with sensors.

NAO is an autonomous, programmable, and medium-sized humanoid robot. Tactile feedback is used in the problem domain related to touch-triggered withdrawal reflexes. This contributes to a safer human–robot interaction [34]. The target was to cover the hands and the upper arms.

In order to implement the artificial skin on the robots, this general procedure has to be followed:

1) identification of the part to be covered [see Fig 2(a)]. If no computer-aided-design (CAD) model is available, obtain the shape with a 3-D laser scanner (as, for example, for the hands of KASPAR);
2) manufacturing of the part (or of a cover) with a 3-D printer (Eden 3-D printer from *Object*) as a support for the sensor. The resulting support looks, for example, like in Fig. 2(b);
3) identification and wiring of the mesh of flexible PCBs that is needed to cover the part [see Fig. 2(c)];
4) bonding of the PCBs on the part with bicomponent glue and the help of a vacuum system [see Fig. 2(d)];
5) covering the PCBs with silicone foam [see Fig. 2(e)]. To this aim, specific purpose-built molds for each part are employed;
6) covering of the silicone foam with a ground plane, as shown in Fig. 2(f), if necessary for this part.

In the following sections, the implementation of the artificial skin for each robot is discussed in detail.

A. Implementation on the Palms of iCub

Before the artificial skin was available, the palm of iCub was made from carbon fiber. As this is a structural part, we decided not to modify it, but instead we added another cover above the carbon fiber part as a support for the sensor: It has a thickness of 1.2 mm and provides space for the CDC chip and the other electronic components (two capacitors for each CDC chip) that are soldered on the PCB. No other particular points had to be considered for the palm and the implementation steps are reported in Fig. 2.

B. Implementation on the Fingertips of iCub

The small size and round shape of the fingertips make a specialized solution necessary. In particular, each fingertip is 14.5-mm long and 13-mm wide and high and has a round shape that resembles a human fingertip. Therefore, a flexible PCB with a custom shape that can be wrapped around an inner solid core had to be designed (see Fig. 3). The structure of the fingertip is illustrated schematically in Fig. 4. To mechanically attach the fingertip to the hand, the last phalange of each digit has a protrusion that fits precisely inside a hole in the inner support of the fingertip. A screw is used to hold the fingertip in place. The screw also fixes a fingernail on top of the fingertip that covers the PCB.

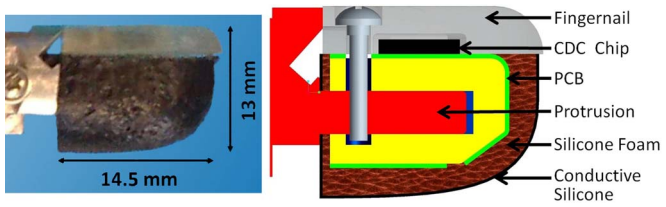

Fig. 4. Fingertip. (Left) Closeup of the fingertip. (Right) Cross section of the fingertip. The flexible PCB is wrapped around the inner support. To mechanically attach the fingertip to the hand, the last phalange of each digit has a protrusion that fits inside a hole in the inner support. A screw is used to secure the fingertip, and in addition, the screw fixes a fingernail on top of the fingertip that covers the PCB. The carbon black layer covers the dielectric made from silicone rubber.

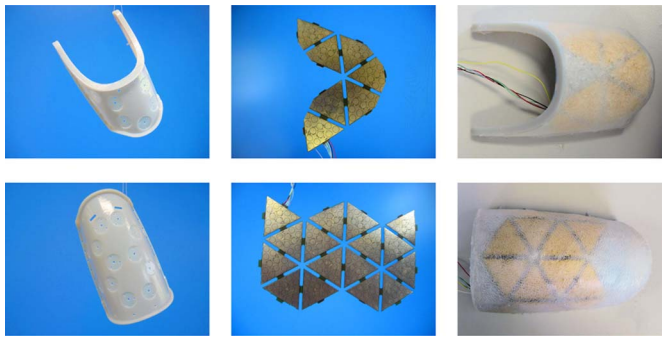

Fig. 5. Process steps for the forearm of iCub. (Upper row) Steps for the upper part of the forearm and (lower row) lower part of the forearm. The first picture in each row shows the support, the middle one shows the mesh of triangles necessary to cover that part, and the right picture presents the result; the triangles are bonded to the support and are covered by soft dielectric foam.

For the fingertips, we use a self-made mixture of silicone CAF4 from *Rhodia-Silicones* and carbon-black particles Vulcan XC72 from *Cabot* as a conductor on top of the silicone foam. It conforms more easily to the round shape of the fingertip than the Lycra-like material. For more details, see [35]. To protect the conductive silicone layer, we spray a thin layer of silicone glue (Sil-Poxy from *Smooth-On*) above it.

As we are using an I^2C serial bus, only four wires have to be connected to the PCB. They travel along the sides of the fingers to small boards at the back of the hand. These boards relay the data from all five fingertips (and the four triangular modules in the palm) to one MTB, which is located in the forearm of iCub.

C. Implementation on the Forearms of iCub

For the two parts that constitute the lower arm, we decided to integrate the skin directly into the cover; therefore, new covers were designed. The production steps are the same as for the palm and are illustrated in Fig. 5. In Figs. 6 and 7, we show the iCub arm covered with artificial skin. Each arm has 384 sensing points: 23 PCBs in the forearm, four in the palm, and five in the fingertips, with 12 sensing points each.

D. Implementation on KASPAR

To obtain a human-like appearance, a child-sized mannequin was used as the basis for KASPAR. The retention of this natural appearance is important to encourage children to touch the robot.

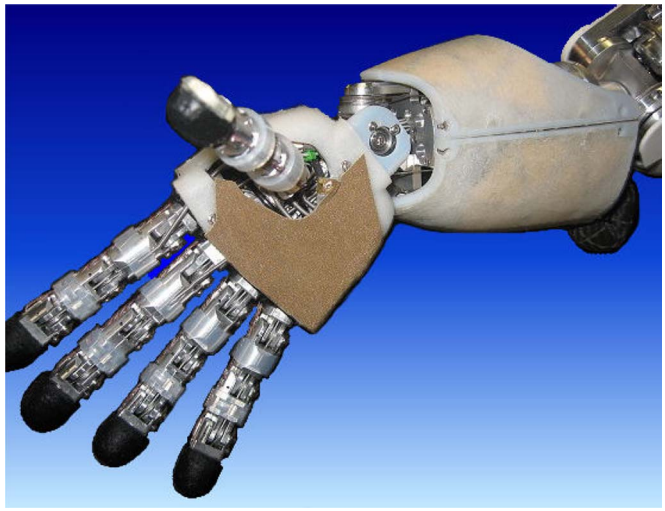

Fig. 6. iCub hand and forearm. The hand has 108 sensitive zones based on our skin technology. In particular, the palm has a skin with four triangular modules, and each fingertip has 12 taxels. The forearm includes 276 contact points.

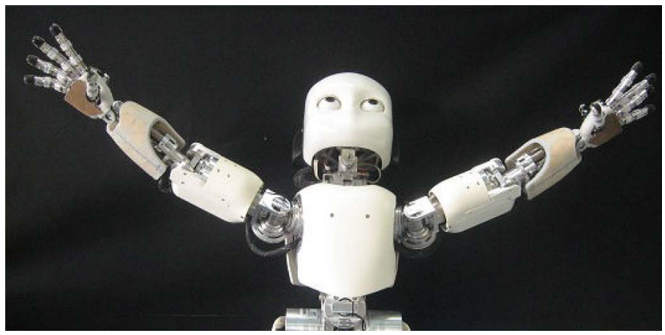

Fig. 7. iCub covered with artificial skin. Each arm has 384 sensing points: 23 PCBs in the forearm, four in the palm, and five in the fingertips, with 12 sensing points each. Note that the artificial skin requires few wires, which can all be routed inside the robot.

Therefore, the hands have been covered with colored silicone foam (see Fig. 8). For the other parts (i.e., cheeks, torso, upper arms, and feet), we did not take the human-like appearance into consideration, because these parts are covered by clothes in the final setup of KASPAR. Moreover, as the robot will interact only with humans, the silicone foam was not covered with a ground plane. We rebuilt the upper and lower arms with the 3-D printer. Because of cost constraints, for the cheeks, torso, and feet, we used the original parts, which do not include the shallow holes for the electrical components. This results in a less smooth, but nevertheless stable, attachment. In addition, no special molds were designed, but instead, standard skin patches were attached to the surface [see Fig. 8(e)]. In total, KASPAR incorporates ten MTB boards and 68 triangles that correspond to 816 contact points.

E. Implementation on NAO

For NAO, the goal was to sensorize the forearms and the upper arms. Therefore, we designed six covers (two for each forearm and one for each upper arm). Fig. 9 shows the steps to cover NAO's forearm with skin. NAO has 18 triangles that

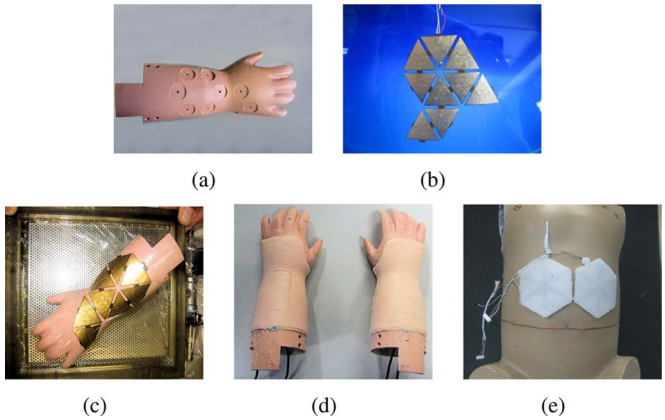

Fig. 8. Sensors for the hands and torso of KASPAR. (a) New hand rebuilt with 3-D printer and (b) triangles. (c) Triangles are glued to the hand. (d) Finished hands: The triangles are covered by colored silicone foam. (e) Standard skin patches are used for the torso.

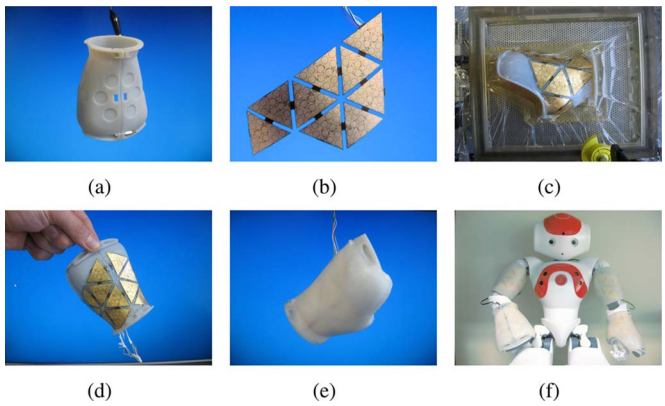

Fig. 9. Steps for implementing the skin on NAO's hands. (a) Two parts of the cover for NAO's forearm. (b) Triangles for one half of the forearm. (c) PCBs are glued to the cover. (d) Cover with the PCBs. (e) Silicone foam has been molded onto the forearm. (f) Final result.

correspond to 216 contact points for each lower arm and nine triangles that correspond to 108 contact points for each upper arm.

V. Calibration of Noise, Touch Detection, and Thermal-Drift Compensation

A. Calibration of Measurement Noise

Out of the 16 measurement bits that the CDC chips can provide, in our implementation, usually, 3 bits are affected by noise, and 5 bits are out of range. Therefore, we use only 8-bit measurements. In these remaining 8 bits, the sensor measurements usually oscillate between two neighboring values (not only due to noise but due to the delta–sigma analog-to-digital conversation used by the CDC as well). Yet, in few taxels, the noise can be up to ± 3 measurement units of the baseline. We could trace the cause of this back to the soldering quality of the CDC: If a pin is not perfectly aligned with its soldering pad, the sensor measurements include more noise. In Section VI-E, we will discuss that in the palm that we used for our tests the noise was very low for all taxels.

Due to these differences between the taxels, we calibrate each taxel individually before using the sensor. In the calibration phase, which lasts a couple of seconds, we calculate the baseline and the 95% percentile of the sensor measurements for each taxel. The baseline is the average measurement during the calibration phase.

B. Touch Detection

The touch-threshold (if the value is larger or equal than this, we define that the taxel has come in contact with an object) is the 95% percentile plus a safety margin (we empirically set this safety margin as two measurement units). This margin allows small fluctuations in the measurements to occur and be detected by the drift-compensation algorithm (as described in the next section) as well as accounts for additional noise that was not present in the calibration phase. With this safety margin, we could observe practically no false-positive touch detections during our experiments.

C. Thermal-Drift Compensation

In some configurations, capacitive pressure sensors are sensitive to temperature (see, for example, [3]). The resulting thermal drift affects the accuracy of the pressure sensor in practical applications. Many methods for drift compensation have been studied, for example, in [36]. We use a simple method that was inspired by the compensation algorithm utilized in the CDC chip [3]. It is fast enough to be implemented in real time:

MAX_COMP_PER_SECOND = 0.1;
CHANGE = MAX_COMP_PER_SECOND / FREQUENCY;
at each timestep, for each taxel$_j$, if taxel$_j$ not touched:
  measurement$_j$ $-=$ baseline$_j$;
  if measurement$_j$ > 0.5: baseline$_j$ $+=$ CHANGE;
  if measurement$_j$ < 0.5: baseline$_j$ $-=$ CHANGE.

We adapt the baseline of each taxel in small steps at every timestep. MAX_COMP_PER_SECOND, which is the maximum compensation per second, was set to 0.1 (given in raw measurement units). This value is far higher than the maximum drift per second that we encountered in our experiments, yet is it low enough not to cause big oscillations in the baseline due to noise. We do not change the baseline if the taxel was touched, or if it is within a margin of ± 0.5 of the baseline (given in raw measurement units). We use this margin as the measurements usually oscillate between two neighboring values, as explained above.

The drift compensation was employed in all the following experiments. As a result, we could observe no drift in the sensor measurements (without causing a waveform distortion, a phase shift, or a transient response).

VI. Testing

Here, we present tests that have been performed with the palm of iCub. Moreover, an algorithm to compensate the hysteresis in the sensor measurements is presented.

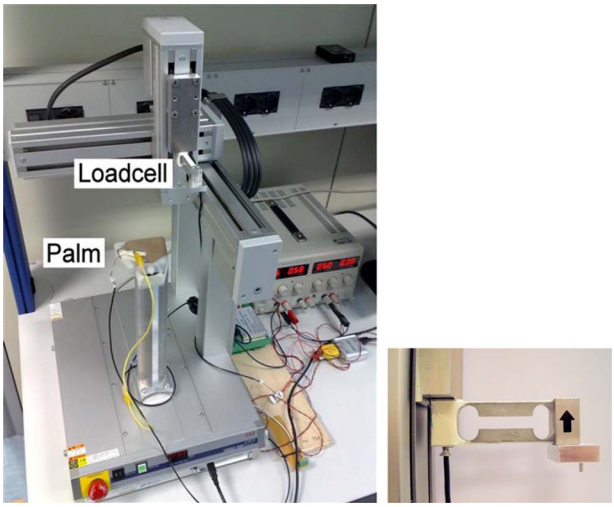

Fig. 10. Test setup. (Left) Test setup that is used to test the characteristics of the sensor. The palm is mounted on a platform. A Cartesian robot (TT-C3-2020 from *IAI*) moves an off-center load cell (0.5 kg AS series, from *Laumas*). (Right) Closeup of the load cell and the probe that pushes against the palm.

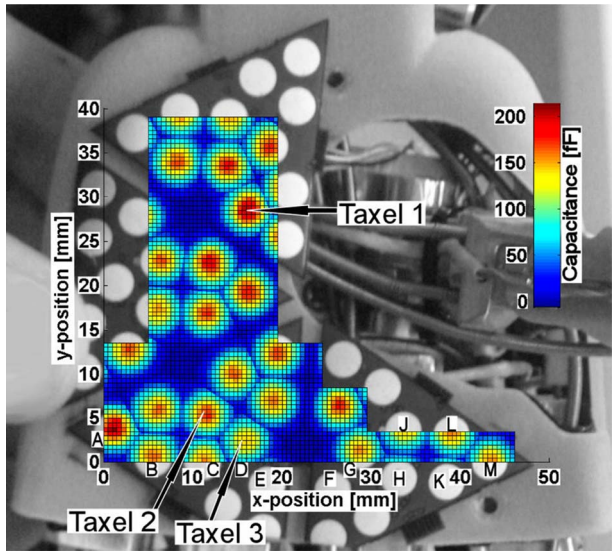

Fig. 11. Sensor response at different positions. We show the superimposed response of all taxels to a certain pressure (i.e., 150–160 kPa). In the background, we show a grayscale picture of the palm (without the silicone foam and the top conductive layer) to demonstrate the correspondence of the sensitive areas to the round pads on the PCBs. For the illustration, an old version of the PCBs is used, which better highlights the electrode areas.

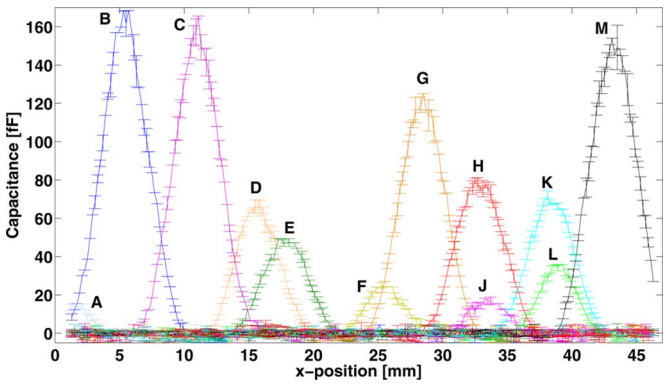

Fig. 12. Spatial resolution of the palm. The probe (with 3-mm diameter) is pushing the palm at different positions (i.e., 0.2-mm distance to each other) along a straight line (corresponding to Fig. 11, where y-position = 0 mm). We show the average measurement and standard deviation of all taxels in both the triangular modules that the tip crosses. The letters show the correspondence of the activated taxels to the taxels in Fig. 11.

A. Test Setup

To test the capacitive pressure sensor, we use a Cartesian robot (TT-C3-2020 from *IAI*). The robot moves an off-center load cell (0.5 kg AS series, from *Laumas*). At the end of the load cell, cylindrical probes of varying diameter can be attached (see Fig. 10). The Cartesian robot moves the load cell with the probe in the x-, y-, and z-directions, and can therefore push the probe vertically against the palm at different locations. The position of the load cell can be determined via the serial interface of the robot, with a maximum frequency of 25 Hz. Therefore, we collect all measurements with a frequency of 25 Hz. The signal from the load cell is amplified by an AT-10 from *Precise Instruments*. To digitize the signal, we use the same MTB that we also use to send the measurements of the capacitive pressure sensor system to the PC. Therefore, we get synchronized data from the capacitive pressure sensor system and the load cell. The pressure applied to the palm is calculated as the force measured by the load cell divided by the contact area. The measurements of the capacitive pressure sensor system are converted to Farad (i.e., 1 measurement unit = 2.88 fF).

B. Spatial Resolution

We tested the spatial resolution of the sensor in the following way: A metal probe with a 3-mm diameter applied pressure to the palm at different positions, which have a distance of 0.5 mm to each other. We never applied pressure to two adjacent positions one after another, to avoid the influence of hysteresis on the measurements (which we will discuss later), but instead covered the palm in a pattern where one push is 5 mm apart from the next. At each position, the probe moved slowly down and then quickly up, and subsequently changed the position. After we got measurements for each position (which took a couple of hours), we subsequently tested each position a second time, to get more measurements and confirm the stability of the sensor measurements over time. In Fig. 11, we show the response of all the taxels to a certain load; to do this, we filtered the data offline and plot only those values that correspond to a pressure of 150–160 kPa. To avoid the effects of hysteresis we used only the measurements while the probe was moving down. Furthermore, we tested only a part of the surface area, as we can only compare positions where the whole probe touches the palm nearly perpendicular. This is because we want to show the response of all taxels to a certain pressure; yet, if only a part of the probe touches the palm or if the probe is not perpendicular to the palm, the pressure applied to the palm varies, even if the load cell measures the same force. We show the superimposed capacitance of all taxels, and in the background, we show a

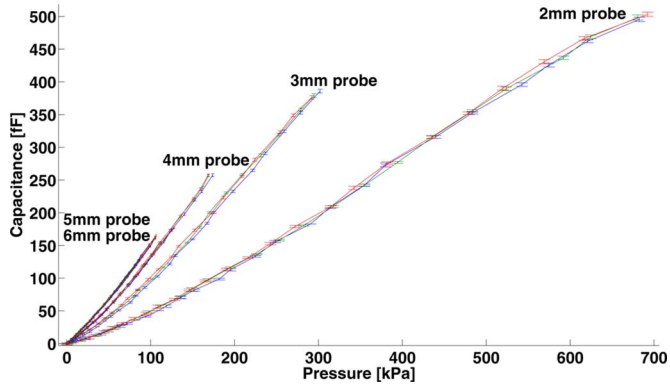

Fig. 13. Response of taxel 2 to varying pressure with different tip sizes. Probes of different sizes were used to push the taxel with varying pressure. We show the average and standard deviation of the first second of measurements.

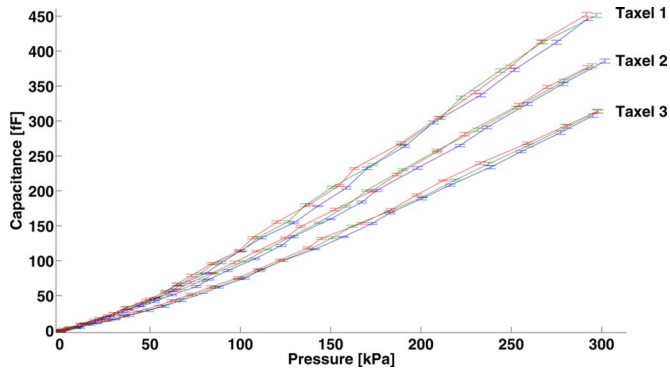

Fig. 14. Response of taxels 1, 2, and 3 to varying pressure with a 3-mm tip. A 3-mm probe was used to push the taxel with varying pressure. We show the average and standard deviation of the first second of measurements.

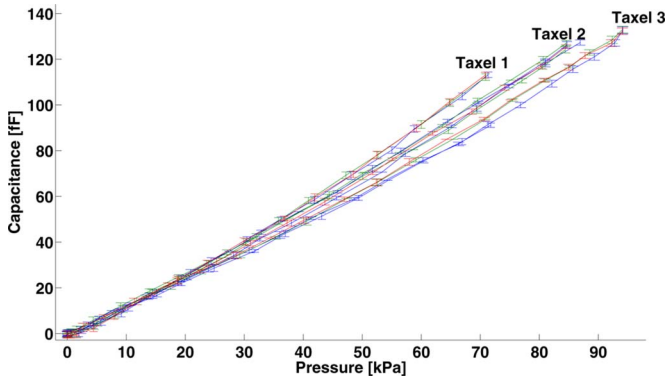

Fig. 15. Response of taxels 1, 2, and 3 to varying pressure with a 6-mm tip. A 6-mm probe was used to push the taxel with varying pressure. We show the average and standard deviation of the first second of measurements.

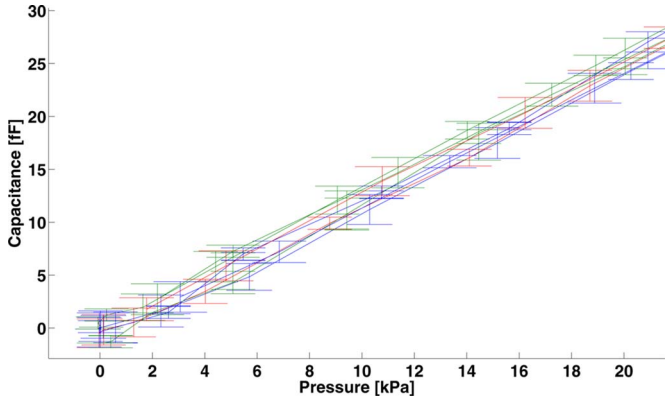

Fig. 16. Response of taxel 2 to varying pressure with a 6-mm tip. A 6-mm probe was used to push the taxel with varying pressure. We show the average and standard deviation of the first second of measurements.

picture of the PCBs to demonstrate the correspondence of the sensitive areas to the round pads on the PCBs.

In Fig. 12, we present the results of another experiment in which the y-position of the probe is always zero and the x-positions are 0.2 mm from each other. The results show that the taxels respond in a bell-shaped curve that little or no crosstalk occurs and that the responsive zones overlap. We conclude that the sensor can be used to localize where pressure is applied to it.

C. Contact Area

We investigated the influence of the contact area on the measurements. The probe was placed above the center of the taxel 2 (see Fig. 11). The probe moved down to a certain depth as fast as possible, remained there, and after 2 s, it moved up again to the noncontact position. The probe remained in this position for 20 s to minimize the effects of hysteresis on the measurements. After that it moved down again, this time 0.1 mm deeper than before, and the whole process was repeated until the probe had pushed to the deepest defined point. We conducted these experiments with probes of different sizes, in particular, 2, 3, 4, 5, and 6 mm. The probes up to 5 mm were made from aluminum, and the one with 6 mm diameter was made from plastic (with our sensor, the material does not influence the measurements). For each probe size, we conducted three consecutive cycles. In Fig. 13, we plot the average and standard deviation of the first second of capacitance measurements. The pressure was calculated as the force measured by the load cell divided by the contact area.

As was expected, for the same pressure, the sensor measurements are higher while using probes of a bigger diameter. Yet, the results from the probe sizes of 5 and 6 mm overlap and cannot be distinguished; therefore, it can be concluded that the response of the sensor is without regard of the probe size, starting from 5 mm diameter.

D. Difference in Response Between Different Taxels

When closely investigating the results of Fig. 11, it can be seen that the maximum activation for different taxels is different. In particular, the maximum capacitance of taxel 1 is 200.5 fF, taxel 2 is 165.5 fF, and taxel 3 is 139 fF. Therefore, the maximum measurements of taxel 1 are nearly 1.5× higher than those of taxel 3. We investigated this further and conducted an experiment similar to Section VI-C. We pushed the palm with a 3-mm probe at different depths, again waiting 20 s in between. In Fig. 14, we show the results for the three different taxels indicated in Fig. 11 (these correspond to a low-, medium-, and high-response taxel). The results in Fig. 14 correspond to the

ones given in Fig. 11: For taxel 1, the response is higher than for the others, and taxel 3 has the lowest response. This is probably due to the varying density of the silicone foam.

Yet, it is interesting to note that up to a certain pressure, the responses overlap. Therefore, we repeated the experiment with a probe size of 6 mm and with a lower maximum pressure (the force we applied is nearly the same, but the contact area is bigger) (see Fig. 15). While there are still differences between the taxels, they are small. We concluded that while there are differences between the taxels, they become increasingly negligible with smaller pressure.

E. Noise, Stability, and Sensitivity

All the results presented thus far show that there is low noise in the 8-bit measurements that we are using; the standard deviations as well as the differences between the repetitions are low. Moreover, the response of the sensor is stable: even though it took many hours to collect the results, given a certain probe size and a certain location, the measurements of all testing cycles overlap.

In Fig. 16, we plot the results that we collected in Section VI-C and VI-D for taxel 2 (see Fig. 11) with a probe size of 5 and 6 mm, focusing on small pressure. We conclude that pressure differences of about 5 kPa can be reliably detected.

F. Calibration, Part 1: Nonlinearity

The response of the sensor is slightly nonlinear, and we used a quadratic function to convert the sensor measurements $S(t)$ at time t (in femtofarad) to pressure $C(t)$ (in kilopascal) (without taking into account the relaxation of the silicone foam, which we will discuss later)

$$C(t) = aS(t)^2 + bS(t) \tag{1}$$

with $a = -0.001132$, and $b = 0.8141$. To compute these values, we used all the data described in the previous sections collected for taxel 2 with a 5- or 6-mm probe. The quadratic term is quite small and the sensor can be assumed to respond linear to changing pressure if smaller precision is necessary.

G. Calibration, Part 2: Viscoelastic Behavior

So far we have applied pressure to the sensor only for short time intervals. In such short time frames, the pressure can be assumed to be constant if the position of the probe is steady. However, when the sensor is loaded for extended time periods, the pressure cannot be assumed to be constant anymore. This is due to the viscoelasticity of the silicone foam. Viscoelastic materials have not only an immediate elastic response but a time-dependent viscous behavior as well: When the strain is held constant, the stress decreases with time (i.e., relaxation); if cyclic loading is applied, hysteresis (i.e., a phase lag) occurs. Therefore, if we want to calculate the applied pressure out of the sensor measurements, we have to take this time-dependent behavior into account. Many models exist to describe the relaxation behavior of viscoelastic materials [37]. In our case, we assume that the sensor measurements $S(t)$ correspond to strain. We use $C(t)$ instead of $S(t)$, as it takes into account the nonlinear behavior of our sensor. Therefore, $P_{\text{cal}}(t)$, which is the calculated pressure, is given by

$$P_{\text{cal}}(t) = C(t) - \text{relax}(t) \tag{2}$$

where $\text{relax}(t)$ is the time-dependent relaxation. In a first approximation, it can be said that the stress decays exponentially with time. Suppose, due to a constant strain ε, we get a constant value for $C(t) = C$; then, $\text{relax}(t)$ is given by

$$\text{relax}(t) = C\beta(1 - e^{-t/\tau}) \tag{3}$$

where β is a scaling factor, and the relaxation approaches asymptotically the final value $C\beta$. The time constant τ is the time it takes to reach $1 - 1/e \approx 63.2\%$ of the final value.

Now, let us consider a variable $C(t)$ and write it as a sum of $\Delta C_1, \Delta C_2, \ldots$, at times $T_1, T_2, \ldots$, respectively. According to Boltzmann's superposition principle, the relaxation is a function of the entire history of the sensor. The total relaxation is, therefore, given by

$$\text{relax}(t) = \sum_i \Delta C_i \beta(1 - e^{-(t-T_i)/\tau}) \tag{4}$$

where ΔC_i is the incremental change of C at time T_i. In our experimental setup, the strain, and as consequence of that, C changes slowly and monotonically, even if the Cartesian robot is static. This is because the load cell is slightly compliant, and the tip changes its position as the silicone foam is relaxing. A similar effect can be expected if the robot-actuation system is compliant or the object that is in contact with the skin is soft. On the other hand, the sensor measurements also vary slightly at nearly every time step due to the digitization and the noise, as discussed before; the resulting changes in C should not be considered; otherwise, the algorithm becomes computationally expensive. We, therefore, substitute ΔC_i with ΔD_i, which is obtained with a moving-average and a threshold: Every second we compute the average of $C(t)$ and check whether it is more than 1.5 kPa different than the sum of all ΔD_i so far, in which case, we add a new ΔD_i.

Moreover, we observed that while unloading (i.e., ΔD is negative in this case), the relaxation term has slower dynamics, and therefore, different parameters should be used in this case. This phenomenon has been described many times in literature, for example, [38]. Therefore, we use β_l and τ_l when ΔD is positive and β_u and τ_u when ΔD is negative.

Finally, the model, as described in (3), represents the relaxation behavior of viscoelastic materials only to a first approximation, which can be better described with the superposition of many exponential functions. In our case, we found that a sum of three exponential functions gives satisfying results. Therefore, we have three β_l, τ_l, β_u, and τ_u each. The final result is given by

$$\begin{aligned}\text{relax}(t) = &\sum_{\Delta D_i > 0} \sum_{k=1}^{3} \Delta D_i \beta_{l_k} (1 - e^{-(t-T_i)/\tau_{l_k}}) \\ &+ \sum_{\Delta D_i < 0} \sum_{k=1}^{3} \Delta D_i \beta_{u_k} (1 - e^{-(t-T_i)/\tau_{u_k}}).\end{aligned} \tag{5}$$

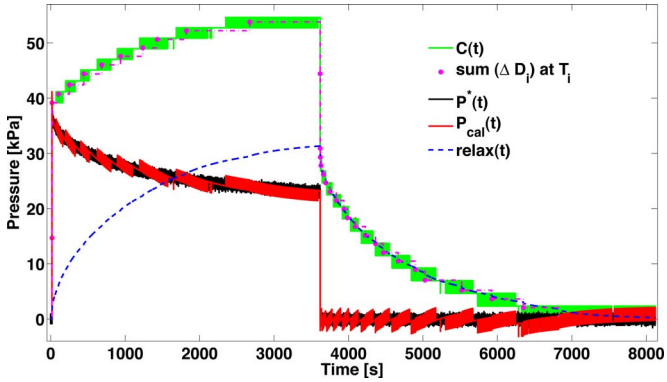

Fig. 17. Compensation of the relaxation of the silicone foam. We applied pressure for 1 h. $C(t)$ corresponds to the uncorrected sensor measurements ΔD_i to their stepwise approximation, relax(t) is the correction term, and $P_{\text{cal}}(t)$ are the corrected measurements: $P_{\text{cal}}(t) = C(t) - \text{relax}(t)$. $P^*(t)$ is the pressure calculated from the load cell, and there is a clear correspondence to $P_{\text{cal}}(t)$.

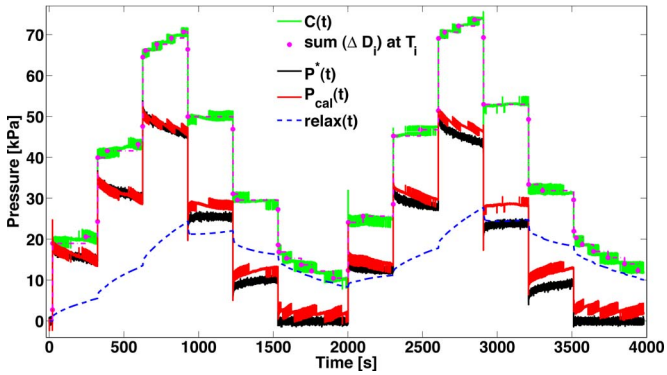

Fig. 18. Compensation of the relaxation of the silicone foam. We applied multistep, cyclic loading. $C(t)$ is the uncorrected sensor measurements, ΔD_i is stepwise approximation, relax(t) is the correction term, and $P_{\text{cal}}(t)$ are the corrected measurements: $P_{\text{cal}}(t) = C(t) - \text{relax}(t)$. $P^*(t)$ is the pressure calculated from the load cell, and there is a clear correspondence to $P_{\text{cal}}(t)$.

TABLE I
PARAMETERS TO CALCULATE THE RELAXATION

Parameter	Value [s]	Parameter	Value
τ_{l_1}	2.17	β_{l_1}	0.0649
τ_{l_2}	117.42	β_{l_2}	0.0968
τ_{l_3}	909.04	β_{l_3}	0.4376
τ_{u_1}	3.22	β_{u_1}	0.1500
τ_{u_2}	202.28	β_{u_2}	0.1548
τ_{u_3}	750.91	β_{u_3}	0.2983

To get the parameters, we pushed a 6-mm probe with maximum speed against the palm and kept it in stationary position for 1 h. Subsequently, we quickly unloaded the sensor and collected further 75 min of data. The goal was to find the parameters so that $P_{\text{cal}}(t)$ matches $P^*(t)$, which is the pressure given by the load-cell measurements divided by the contact area. We first calculated the three β_l and τ_l and used the data between the first stress and the first release. Afterward, we used the data starting at the unloading until the end of the measurements, subtracted the relaxation due to the ΔD that happened before (we used the parameters that we had just determined), and calculated the three β_u and τ_u for unloading. The result can be seen in Fig. 17. The parameters are reported in Table I.

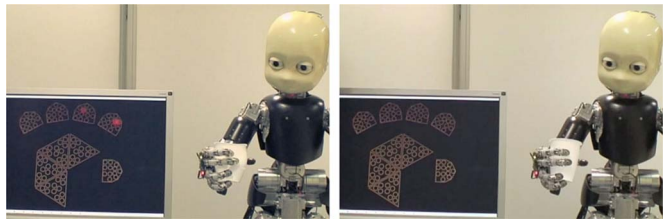

Fig. 19. iCub is grasping a fragile plastic cup. (Left) Without tactile feedback, iCub crushes the cup. (Right) With tactile feedback, it grasps the cup without deforming it. In addition, the resulting activation in the fingertips is shown; with feedback control, it is so low that it is not visible. This visualization also shows the schematic representation of how the sensors are distributed on the fingers and the palm. The pictures are taken from a video that can be found in [39].

We subsequently tested whether our model works by calculating $P_{\text{cal}}(t)$ for other datasets, using the parameters that we have just found. The results were generally satisfying. In Fig. 18, we present the most-difficult scenario and the worst result we obtained: In this experiment, we used a different maximum pressures, different time periods, and multistep and cyclic loading. Moreover, the total time of pressure applied to the sensor is far higher than we expect it to be in the humanoid robots. In this case, we could see slight differences in $P_{\text{cal}}(t)$ and $P^*(t)$. We could observe this effect, in general, when applying pressures higher than the one in our original dataset. Nevertheless, we concluded that this model is good enough for our purposes.

Finally, we want to point out that the initial response of the capacitive sensor to a change of displacement of the probe is fast: There is no delay between the initial change of the measurements of the capacitive sensor and the load cell, and initially, $C(t)$ is nearly equal to $P^*(t)$. This is further demonstrated by the correspondence of the measurements in Section VI-B and D, which were obtained in dynamic and static conditions, respectively. Yet, we did not measure the delay due to the MTB and the subsequent CAN bus.

VII. GRASPING EXPERIMENTS

In [29], we grasped three different objects with a preprogrammed behavior, and could show that the sensor measurements are stable over time and can be used to detect touch. In the experiment described here, we use the feedback provided from the sensors to grasp a fragile object, in particular, a plastic cup. In the video [39], we first show that the iCub can crush the cup. Subsequently, with the help of the tactile sensors it grasps the same cup gently without deforming it (see Fig. 19).

At start-up iCub calibrates its sensors: it opens the hand completely and collects measurements for 5 s. To compensate for drift and to detect whether an object touches the skin, we use the algorithm, as described in Section V. After the calibration, we place a plastic cup in the hand of iCub and start the grasping. First, iCub grasps the cup without tactile feedback, and afterwards with tactile feedback. The algorithm is simple: For each finger, when one of the taxels in the fingertips detects touch, the movement stops; otherwise, a closing movement is performed. In Fig. 20, we show the resulting activation in all the taxels that reached their touch threshold during the experiment.

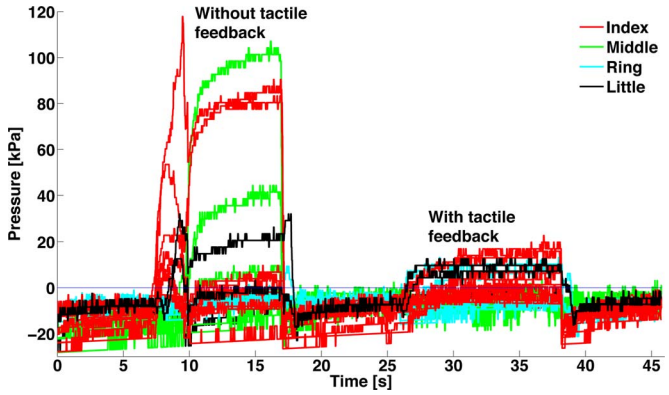

Fig. 20. Average activation of all taxels that reached their touch-threshold while iCub is grasping a cup with and without tactile feedback. We subtracted from each taxel its individual baseline (which includes the drift compensation) and its individual touch threshold; therefore, a taxel detects a touch if it measures more than 0 fF. The taxels are clearly more activated when grasping the cup without tactile feedback.

The taxels are clearly more activated while iCub is crushing the cup than while it is grasping it gently. We performed ten such grasps, and in each case, iCub grasped the cup without deforming it.

VIII. Conclusion and Future Work

We have presented a sensorized skin system for humanoid robots that incorporates capacitive sensors. The skin is modular and can be easily customized to cover nonflat surfaces; to demonstrate this, we have shown the sensorization of three different robots, which all have different sizes, shapes, and purposes. Hysteresis and thermal drift are problems that commonly affect capacitive sensors. To overcome these limitations, we have implemented simple algorithms to compensate for drift and hysteresis of our sensor. The sensor has good performance in terms of sensitivity and spatial resolution. This is further demonstrated by experiments on the robot iCub that show that the skin allows a fragile object to be grasped without deforming it. Future work will focus on evaluating the sensor's robustness and usefullness for a wider range of robotic tasks.

References

[1] J. Webster, *Tactile Sensors for Robotics and Medicine*. New York: Wiley, 1988.
[2] M. H. Lee and H. R. Nicholls, "Tactile sensing for mechatronics: A state of the art survey," *Mechatronics*, vol. 9, pp. 1–31, 1999.
[3] Analog Devices, Inc. (2008). AD7147 technical datasheet [Online]. Available: http://www.analog.com/static/imported-files/Data_Sheets/AD7147.pdf
[4] Y. Ohmura, Y. Kuniyoshi, and A. Nagakubo, "Conformable and scalable tactile sensor skin for curved surfaces," in *Proc. IEEE Int. Conf. Robot. Autom.*, 2006, pp. 1348–1353.
[5] Y. Ohmura and Y. Kuniyoshi, "Humanoid robot which can lift a 30kg box by whole body contact and tactile feedback," in *Proc. IEEE/RSJ Int. Conf. Intell. Robots Syst.*, 2007, pp. 1136–1141.
[6] T. Mukai, M. Onishi, S. Hirano, and Z. Luo, "Development of the tactile sensor system of a human-interactive robot "RI-MAN"," *IEEE Trans. Robot.*, vol. 24, no. 2, pp. 505–512, Apr. 2008.
[7] T. Asfour, K. Regenstein, J. Schroder, and R. Dillmann, "ARMAR-III: A humanoid platform for perception-action integration," presented at Int. Workshop Human-Centered Robot. Syst., Munich, Germany, 2006.
[8] I. Mizuuchi, T. Yoshikai, T. Nishino, and M. Inaba, "Development of musculoskeletal humanoid Kotaro," in *Proc. IEEE Int. Conf. Robot. Autom.*, 2006, pp. 82–87.
[9] T. Tajika, T. Miyashita, and H. Ishiguro, "Automatic categorization of haptic interactions-what are the typical haptic interactions between a human and a robot?," in *Proc. IEEE-RAS Int. Conf. Humanoid Robots (Human.)*, 2006, pp. 490–496.
[10] T. Minato, Y. Yoshikawa, H. Ishiguro, and M. Asada, "CB2: A child robot with biomimetic body for cognitive developmental robotics," in *Proc. IEEE-RAS 7th Int. Conf. Human. Robots (Human.)*, 2007, pp. 557–562.
[11] T. Sekitani and T. Someya, "Stretchable, large-area organic electronics," *Adv. Mater.*, vol. 22, no. 20, pp. 2228–2246, 2010.
[12] H. Alirezaei, A. Nagakubo, and Y. Kuniyoshi, "Development of a highly stretchable tactile sensor with easy wearability," presented at Human. Workshop: Tactile Sens. Human.—Tactile Sens. Beyond, 2009, Paris, France.
[13] T. Mouri, H. Kawasaki, K. Yoshikawa, J. Takai, and S. Ito, "Anthropomorphic robot hand: Gifu Hand III," in *Proc. Int. Conf. Control, Autom. Syst.*, Oct. 2002, pp. 1288–1293.
[14] G. Cannata and M. Maggiali, "Design of a tactile sensor for robot hands," *Sensors: Focus on Tactile Force and Stress Sensors*, Rijeka, Croatia: In-Tech, 2008, pp. 271–288.
[15] L. Natale and E. Torres-Jara, "A sensitive approach to grasping," in *Proc. 6th Int. Conf. Epigenet. Robot.*, 2006, pp. 1–8.
[16] Shadow Hand Company. (2008). Shadow dexterous hand [Online]. Available: www.shadowrobot.com/hand/
[17] T. B. Martin, R. O. Ambrose, and J. M. Butzer, "Tactile gloves for autonomous grasping with the NASA/DARPA robonaut," in *Proc. IEEE Int. Conf. Robot. Autom.*, 2004, pp. 1713–1718.
[18] Z. Chu, P. M. Sarro, and S. Middelhoek, "Silicon three-axial tactile sensor," *Sens. Actuat. A*, vol. 54, pp. 505–510, 1996.
[19] B. L. Gray and R. S. Fearing, "A surface micromachined microtactile sensor array," in *Proc. Int. Conf. Robot. Autom.*, 1996, pp. 1–6.
[20] R. J. D. Souza and K. D. Wise, "A very high density bulk micromachined capacitive tactile imager," in *Proc. Int. Conf. Solid-State Sens. Actuat., Transducers*, 1997, pp. 1473–1476.
[21] J. Ulmen and M. Cutkosky, "A robust, low-cost and low-noise artificial skin for human-friendly robots," in *Proc. IEEE Int. Conf. Robot. Autom.*, 2010, pp. 4836–4841.
[22] K. Wada and T. Shibata, "Social effects of robot therapy in a care house—Change of social network of the residents for two months," in *Proc. IEEE Int. Conf. Robot. Autom.*, 2007, pp. 1250–1255.
[23] P. A. Schmidt, E. Mael, and R. P. Wurtz, "A sensor for dynamic tactile information with applications in human–robot interaction & object exploration," *Robot. Auton. Syst.*, vol. 54, pp. 1005–1014, 2006.
[24] Pressure Profile Systems Inc. (2010). Pps-products [Online]. Available: http://www.pressureprofile.com/products.php
[25] H. Iwata, "Design of human symbiotic robot TWENDY-ONE," in *Proc. IEEE Int. Conf. Robot. Autom.*, 2009, pp. 580–586.
[26] M. Maggiali, G. Cannata, P. Maiolino, G. Metta, M. Randazzo, and G. Sandini, "Embedded distributed capacitive tactile sensor," in *Proc. Mechatron.*, 2008, pp. 1–5.
[27] A. Schmitz, M. Maggiali, L. Natale, B. Bonino, and G. Metta, "A tactile sensor for the fingertips of the humanoid robot iCub," in *Proc. IEEE/RSJ Int. Conf. Intell. Robots Syst.*, 2010, pp. 2212–2217.
[28] A. Schmitz, M. Maggiali, L. Natale, and G. Metta, "Touch sensors for humanoid hands," in *Proc. 19th IEEE Int. Symp. Robot Human Interact. Commun.*, 2010, pp. 691–697.
[29] A. Schmitz, U. Pattacini, F. Nori, L. Natale, G. Metta, and G. Sandini, "Design, realization and sensorization of a dextrous hand: The iCub design choices," in *Proc. IEEE-RAS Int. Conf. Human. Robots (Human.)*, 2010, pp. 186–191.
[30] R. Dahiya, G. Metta, M. Valle, and G. Sandini, "Tactile sensing: From humans to humanoids," *IEEE Trans. Robot.*, vol. 26, no. 1, pp. 1–20, Feb. 2010.
[31] G. Metta, D. Vernon, L. Natale, F. Nori, and G. Sandini, "The iCub humanoid robot: an open platform for research in embodied cognition," presented at IEEE Workshop Perform. Metrics Intell. Syst., San Jose, CA, 2008.
[32] B. Argall, E. Sauser, and A. Billard, "Tactile feedback for policy refinement and reuse," in *Proc. 9th IEEE Int. Conf. Dev. Learning*, 2010, pp. 7–12.
[33] K. Dautenhahn, C. L. Nehaniva, M. L. Waltersa, B. Robins, H. Kose-Bagcia, N. A. Mirzaa, and M. Blow, "KASPAR—A minimally

expressive humanoid robot for human–robot interaction research," *Appl. Bion. Biomech.*, vol. 6, no. 3, pp. 369–397, 2009.
[34] T. S. Dahl and A. Palmer, "Touch-triggered protective reflexes for safer robots," in *Proc. Int. Symp. New Front. Human-Robot Interact*, 2010, p. 7.
[35] A. Schmitz, M. Maggiali, M. Randazzo, L. Natale, and G. Metta, "A prototype fingertip with high spatial resolution pressure sensing for the robot iCub," in *Proc. IEEE-RAS Int. Conf. Human. Robots (Human.)*, 2008, pp. 423–428.
[36] Z. Zeng, L. Zheng, and D. Ling, "A compensation method of the offset thermal drift of sensor using the neural network algorithm," in *Proc. ICSP*, 2008, pp. 1716–1718.
[37] W. N. Findley, J. S. Lai, and K. Onaran, *Creep and Relaxation of Nonlinear Viscoelastic Materials*. New York: Courier Dover, 1989.
[38] M.-A. Lacasse, V. Duchaine, and C. Gosselin, "Characterization of the electrical resistance of carbon-black-filled silicone: Application to a flexible and stretchable robot skin," in *Proc. IEEE Int. Conf. Robot. Autom.*, 2010, pp. 4842–4848.
[39] A. Schmitz. (2010). iCub grasps a fragile plastic cup with its tactile sensors. youtube, robotcub's channel [Online]. Available: www.youtube.com/watch?v=jQfX2SyxxXo

Alexander Schmitz received the Master's degree in cognitive science (with honors) from the University of Vienna, Vienna, Austria, in 2007. He is currently working toward the Ph.D. degree as part of a joint location program with the University of Sheffield, Sheffield, U.K., and with the Italian Institute of Technology, Genova, Italy.

He was engaged in the development of a tactile system for the hands of the humanoid robot iCub. His research for Master's thesis was performed with the Artificial Intelligence Laboratory, University of Zurich, Zurich, Switzerland.

Perla Maiolino received the M.S. degree in robotics and automation and the Ph.D. degree in robotics from the University of Genova, Genova, Italy, in 2006 and 2010, respectively.

She is currently a Postdoctoral Researcher with the Mechatronic and Control Laboratory, Department of Communication, Computer, and System Sciences, University of Genova. Her current research interests include materials and in the design of technological solutions related to the development of distributed tactile sensors for robots.

Marco Maggiali was born in Genova, Italy, in 1980. He received the Comput. Eng. degree from the University of Genova in 2005 and the Ph.D degree in humanoid technologies from the Italian Institute of Technology (IIT), Genova, in 2009.

Since 2009, he has been a Research Engineer with IIT. His current research interests include humanoid robots, embedded electronics, and tactile sensing.

Lorenzo Natale received the Electronic Engineering degree (with honors) and the Ph.D. degree in robotics from the University of Genova, Genova, Italy, in 2000 and 2004.

He was with the Laboratory for Integrated Advanced Robotics, University of Genova. Between 2005 and 2006, he was a Postdoctoral Researcher with the Humanoid Robotics Group, Computer Science and Artificial Intelligence Laboratory, Massachusetts Institute of Technology, Cambridge. He is currently a Team Leader with the Italian Institute of Technology, Genova. His current research interests include developmental robotics, sensorimotor learning, and perception in artificial and biological systems, as well as software development and integration in robotics.

Giorgio Cannata received the Laurea degree in electronic engineering from the University of Genova, Genova, Italy, in 1988.

He is currently an Associate Professor of automatic and digital control with the Faculty of Engineering, University of Genova. From 1989 to 1995, he was a Research Scientist with the Naval Automation Institute, Italian National Research Council, where he was engaged in the area of underwater robotics. From 1995 to 1998, he was an Assistant Professor with the Department of Communication, Computer, and System Sciences, University of Genova. His current research interests include humanoid robots, automatic control systems, and control architectures for robotic and mechatronic systems, as well as robotics and robot control theory, control of mechanical systems, and dynamic simulation.

Giorgio Metta received the M.S. degree (Hons.) and the Ph.D. degree, both in electronic engineering, from the University of Genova, Genova, Italy, in 1994 and 2000, respectively.

From 2001 to 2002, he was a Postdoctoral Associate with the Artificial Intelligence Laboratory, Massachusetts Institute of Technology, Cambridge, where he was involved in various humanoid robotic platforms. Since 2005, he has been an Assistant Professor with the Dipartimento di Informatica Sistemistica e Telematica, University of Genova, where he has been teaching courses on anthropomorphic robotics and intelligent systems. Since 2006, he has also been a Senior Scientist with the Robotics, Brain, and Cognitive Sciences Department, Italian Institute of Technology, Genova. His current research interests include biologically motivated humanoid robotics and, in particular, the development of artificial systems that show some of the abilities of natural systems. His research has been developed in collaboration with leading European and international scientists from different disciplines like neuroscience, psychology, and robotics. He is an author or coauthor of more than 200 publications. He has also been engaged as a Principal Investigator and a Research Scientist with several international- and national-funded projects. He has been a Reviewer of international journals and for the FP7 for the European Commission.